

## Article

# Reduction of Typical Diesel NO<sub>x</sub> Emissions by SCR-NH<sub>3</sub> Using Metal-Exchanged Natural Zeolite and SBA-15 Catalysts

Amanda Pontes Maia Pires Alcantara <sup>1</sup>, Mona Lisa Moura de Oliveira <sup>1,\*</sup>, Jesuína Cássia Santiago de Araújo <sup>2</sup>, Rinaldo dos Santos Araújo <sup>3</sup>, Rita Karolinny Chaves de Lima <sup>4</sup>, André Valente Bueno <sup>5</sup>, Maria Eugênia Vieira da Silva <sup>5</sup>, Paulo Alexandre Costa Rocha <sup>5,6,\*</sup> and Enrique Rodríguez-Castellón <sup>7</sup>

<sup>1</sup> Sciences and Technology Center, State University of Ceará, Fortaleza 60714-903, Brazil

<sup>2</sup> Centro Universitário Norte do Espírito Santo, Federal University of Espírito Santo, São Mateus 29932-540, Brazil

<sup>3</sup> Department of Chemical and Environment, Federal Institute of Ceará, Fortaleza 60020-181, Brazil

<sup>4</sup> Institute of Engineering and Sustainable Development, University of International Integration of the Afro-Brazilian Lusophony, Redenção 62790-000, Brazil

<sup>5</sup> Mechanical Engineering Department, Technology Center, Federal University of Ceará, Fortaleza 60020-181, Brazil

<sup>6</sup> School of Engineering, University of Guelph, 50 Stone Rd E, Guelph, ON N1G 2W1, Canada

<sup>7</sup> Department of Inorganic Chemistry, Campus de Teatinos, University of Malaga, 29071 Málaga, Spain

\* Correspondence: mona.lisa@uece.br (M.L.M.d.O.); paulo.rocha@ufc.br (P.A.C.R.)

**Abstract:** In this work, the catalytic performance of clinoptilolite (CLIN) and SBA-15 catalysts, doped with Fe and Cu, was evaluated in the selective catalytic reduction of NO using NH<sub>3</sub> as a reducing agent (SCR-NH<sub>3</sub>). Both Cu-CLIN and Fe-CLIN were obtained by ion-exchange using natural clinoptilolite zeolite originating from the Hrabovec deposit (northeast Slovakia region). Cu-SBA-15 and Fe-SBA-15 were prepared by impregnation into SBA-15 mesoporous synthesized silica. Standard catalytic activity tests were carried out on a bench-scale laboratory apparatus using a reaction mixture of a standard test. GHSV of 48,000 h<sup>-1</sup> was adopted based on the space velocity of a real NH<sub>3</sub>-SCR catalyst for diesel vehicles (100–550 °C). All Cu-doped samples showed better NO conversion values than Fe-doped samples. Clinoptilolite catalysts were more active than those based on SBA-15. Maximum NO conversions of about 96% were observed for Cu-CLIN and Fe-CLIN at 350–400 °C, respectively. Moreover, Fe-CLIN also showed higher stability in the presence of SO<sub>2</sub> and water steam at 350 °C. These results demonstrate the potential of metal-doped natural clinoptilolite to be used as cost-effective catalysts applied to the abatement of NO<sub>x</sub> emissions generated in automotive combustion processes.

**Keywords:** nitrogen oxides emissions; SCR-NO<sub>x</sub>; diesel engines; natural zeolite; clinoptilolite; SBA-15



**Citation:** Alcantara, A.P.M.P.; Moura de Oliveira, M.L.; Santiago de Araújo, J.C.; dos Santos Araújo, R.; Chaves de Lima, R.K.; Bueno, A.V.; Vieira da Silva, M.E.; Costa Rocha, P.A.; Rodríguez-Castellón, E. Reduction of Typical Diesel NO<sub>x</sub> Emissions by SCR-NH<sub>3</sub> Using Metal-Exchanged Natural Zeolite and SBA-15 Catalysts. *Air* **2023**, *1*, 159–174. <https://doi.org/10.3390/air1030012>

Academic Editors: Paola Palestini and Ling Tim Wong

Received: 14 March 2023

Revised: 2 June 2023

Accepted: 28 June 2023

Published: 30 June 2023



**Copyright:** © 2023 by the authors. Licensee MDPI, Basel, Switzerland. This article is an open access article distributed under the terms and conditions of the Creative Commons Attribution (CC BY) license (<https://creativecommons.org/licenses/by/4.0/>).

## 1. Introduction

Environmental legislation dealing with air pollution has become increasingly restrictive, raising the need to develop technologies capable of reducing the rates of harmful gases and solid particles [1]. Most of the atmospheric pollution registered in large urban centers has been attributed to the combustion processes of fossil fuels, mainly those that occur in motor vehicles (compression and spark ignition engines) [2,3]. During these processes, chemical energy is converted into thermal and mechanical energy, producing emissions such as: carbon monoxide (CO), carbon dioxide (CO<sub>2</sub>), sulfur dioxide (SO<sub>2</sub>), nitrogen oxides (NO<sub>x</sub>), non-methane hydrocarbons (NMHC), aldehydes (RCHO), and methane (CH<sub>4</sub>), in addition to particulate matter (PM).

Among the gases generated in diesel engines, NO<sub>x</sub> emissions have received considerable attention [4–6], since they have been associated with the generation of photochemical pollution [7,8].

The technology conventionally used for denitrogenating combustion gases from diesel engines is the selective catalytic reduction of NO<sub>x</sub> (SCR-NO<sub>x</sub>), which uses ammonia (NH<sub>3</sub>) as a reducing agent. Commercial catalysts based on mixed oxides of the V<sub>2</sub>O<sub>5</sub>/WO<sub>3</sub>/TiO<sub>2</sub> (VWT)-type are used in this process [9]. Although vanadium is the metal responsible for the catalytic activity, this commercial catalyst has presented some inevitable disadvantages, such as: high toxicity, narrow operating range (300–400 °C) and it enhances undesirable reactions (oxidation from SO<sub>2</sub> to SO<sub>3</sub>) [10].

Thus, studies have been directed to the development of catalysts that have low toxicity and that are able to operate in the presence of H<sub>2</sub>O and SO<sub>2</sub> and in wide temperature ranges [4,11,12].

Natural and synthetic zeolites have been cited as promising materials for this purpose as they have high hydrothermal stability, adsorption, and cation exchange capacity. These materials have been able to operate under conditions similar to those of the diesel engine (150–450 °C) [4]. Several studies show that zeolites such as ZSM-5, MOR, FER, BEA, and FAU have been used as catalytic supports in SCR-NO<sub>x</sub> processes [13–17]. The active phase (Cu, Fe, Co, Pt, Rh, and Ni) has been incorporated into the support by ion exchange and wet impregnation. Significant differences in the textural, structural, and surface properties of the catalysts have been observed, depending on the method selected for the incorporation of the metallic phase [4,18]. These differences are reflected in the catalysts' activity and stability, when they are subjected to typical reaction conditions (chains rich in H<sub>2</sub>O and SO<sub>2</sub>). Despite the effort that has been made to clarify such behavior, the results are still incipient.

Both the acidity of the support and the metal phase are known to play a determining role in the activity and stability of the catalysts. In a previous study [19], the incorporation of Fe and Cu in the SBA-15 mesoporous material was evaluated. The Cu-SBA-15 catalyst was observed to show increased activity in the low-temperature region, while Fe-SBA-15 effectively worked in a high-temperature region for the SCR-NO<sub>x</sub> process. Some natural zeolites (MOR, FER, and CLIN) already have Cu, V, and Fe in their composition, and tend to have higher performance as catalysts in SCR-NO<sub>x</sub>. Despite the presence of metals in its structure, the incorporation of additional metals is sometimes necessary. Some authors [12] evaluated the water tolerance of mordenite ion-exchanged with H<sup>+</sup> and Cu<sup>2+</sup>, and observed that the Cu<sup>2+</sup> incorporated by ion exchange shows a slower deactivation than the free Cu catalyst. This reveals that the use of natural zeolites, which already have a percentage of active phase naturally incorporated, presents itself as a potential support to be applied in SCR-NO<sub>x</sub>. Among the zeolites that fall into this category, clinoptilolite (CLIN) should be highlighted, due to its simplicity of mining, considerable reserves, and relatively low cost [20,21]. Therefore, the goal of this work is to evaluate the performance of clinoptilolite and SBA-15 catalysts doped with transition metals such as Fe and Cu, in the selective catalytic reduction of NO<sub>x</sub> using ammonia as a reducing agent. Stability tests were performed using a simulated exhaust current from a diesel vehicle (standard test) rich in H<sub>2</sub>O and SO<sub>2</sub>.

## 2. Materials and Methods

### 2.1. Catalysts Preparation

#### 2.1.1. Chemical

The chemicals used in this study include 3-aminopropyltriethoxysilane (99 wt.% APTES, Sigma-Aldrich (St. Louis, MO, USA) <https://www.sigmaaldrich.com>, accessed on 1 March 2023), acetonitrile (≥98 wt.%, Sigma-Aldrich), hydrochloric acid (37 wt.%, Dinâmica <http://www.dinamicaquim.com.br/>, accessed on 1 March 2023), methanol (≥99 wt.%, Sigma-Aldrich), copper(II) nitrate trihydrate (≥98 wt.%, Vetec/Sigma <https://www.sigmaaldrich.com>, accessed on 1 March 2023), iron(III) nitrate nonahydrate (≥98 wt.%, Vetec-Sigma), Pluronic 123 (99 wt.%, P123, Sigma-Aldrich), tetraethyl orthosilicate (TEOS, 98 wt.%, Acros Organics (Waltham, MA, USA) <https://www.acros.com/>, accessed on 1 March 2023), and ethanol (95 wt.%, Vetec/Sigma). The used natural clinoptilolite comes

from the deposit of Hrabovec (region of north-east Slovakia) and was provided by Celta Brazil <https://www.celtabrasil.com.br>, accessed on 1 March 2023.

### 2.1.2. Catalysts Preparation

SBA-15 was synthesized according to the methodology described in the literature [22]. P123, water and 2 M Hydrochloric acid (37%, Vetec/Sigma <https://www.sigmaaldrich.com>, accessed on 1 March 2023) were mixed at 35 °C to yield a homogenous mixture. After stirring for 30 min, TEOS was added gradually and stirring continued for 20 h. The obtained mixture was transferred and sealed in a Teflon autoclave for hydrothermal treatment at 100 °C for 48 h. The resulting precipitate was separated from the liquid phase by filtering and washed with distilled water before drying at 60 °C for 24 h. Template removal was performed by calcination at 500 °C for 6 h. The nominal molar composition for this synthesis was: 1 TEOS: 0.017 P123: 5.85 HCl: 162 H<sub>2</sub>O.

Samples of Cu-SBA-15 and Fe-SBA-15 were prepared by impregnation of the corresponding carrier with ethanolic solutions of Cu(NO<sub>3</sub>)<sub>2</sub> · 3H<sub>2</sub>O and Fe(NO<sub>3</sub>)<sub>3</sub> · 9H<sub>2</sub>O, respectively. Appropriate amounts of the salts were dissolved in ethanol and the support was then added. After stirring for 2 h at room temperature, ethanol was removed by Rotavapor at 70 °C. The samples were dried at 60 °C for 24 h and calcined at 550 °C for 6 h. For all samples, the amount of Cu and Fe was about 2 wt.%.

The natural clinoptilolite (CLI) with general chemical formula of (Na,K,Ca)<sub>4</sub>Al<sub>6</sub>Si<sub>30</sub>O<sub>72</sub> · 24H<sub>2</sub>O, has structural and spectral properties of aluminum silicate. The Si/Al ratio of clinoptilolite zeolites varies from 4.0 to 5.3, with high thermal stability (>550 °C). Thus, natural clinoptilolite-based catalysts were prepared by ion-exchange with aqueous solutions of iron(III) nitrate nonahydrate and copper(II) nitrate trihydrate. The iron and copper loading was 2.0 wt.%. The ion-exchange was carried out at 60 °C using the NH<sub>4</sub><sup>+</sup>-CLIN in contact with the metal salt solutions during 24 h at pH 6. Then, the mixture was filtered, washed with deionized water and dried at 60 °C for 6 h. Finally, the catalysts were calcined at 550 °C for 6 h with a heating rate of 5 °C min<sup>-1</sup>. The detailed preparation method is described elsewhere [23].

### 2.2. Characterization of the Solids

Chemical analyses of copper were carried out by atomic absorption (AA) spectroscopy (iCE 3000 model, Thermo Scientific (Waltham, MA, USA) <https://www.thermofisher.com/br/en/home.html>, accessed on 1 March 2023).

X-ray diffraction profiles of the samples were collected using an EMPYREAN diffractometer, using Cu-K $\alpha$  radiation. The step-scans were taken over the ranges of 2 $\theta$  from 0.8–10° and 5–70° in steps of 0.0167°. The diffraction patterns have been indexed by comparison with the Joint Committee on Powder Diffraction Standards (JCPDS).

The Fourier-transformed infrared spectroscopy (FTIR) measurements of the solids were performed on a Spectrum 100 FT-IR spectrophotometer. Samples were prepared with dilution in KBr and the spectra were recorded in the 400–4000 cm<sup>-1</sup> range.

BET surface area ( $S_{\text{BET}}$ ), pore volume ( $V_p$ ) and pore size distributions ( $D_p$ ) were measured by nitrogen adsorption–desorption isotherms at –196 °C in a Micromeritics ASAP 2420 instrument. Previously, samples were degassed under vacuum for 24 h at 90 °C. The surface area was estimated from Brunauer–Emmett–Teller (BET) model. The mesopore size distributions were obtained using Barrett–Joyner–Halenda method (BJH). An entire isotherm is needed for one to calculate the pore size distribution of the support and catalyst [24–27].

Pyridine-infrared (IR) spectra were recorded on a Spectrum 100 FT-IR spectrophotometer. Prior to pyridine adsorption, samples (ca. 15 mg) were pressed into pellets, treated in situ at 350 °C for 1 h in N<sub>2</sub> flow (5 mL min<sup>-1</sup>), exposed to pyridine vapor at 25 °C, and then outgassed at 100 °C. The concentration of both types of acid sites (Brønsted and Lewis) were estimated from their integrated absorption at 1550 cm<sup>-1</sup> and 1450 cm<sup>-1</sup>, using

the extinction coefficients obtained in a previous study [28],  $EB = 0.73 \text{ cm } \mu\text{mol}^{-1}$  and  $EL = 1.11 \text{ cm } \mu\text{mol}^{-1}$  for Brönsted and Lewis sites, respectively.

### 2.3. Catalytic Test

Catalytic activity measurements were performed in a fixed-bed quartz microreactor (8 mm i.d.) using 150 mg of catalyst. All catalysts were pelletized with a particle size of 0.25–0.50 mm. The activities of the prepared catalysts (i.e., based in metal-SBA-15 and metal-CLIN) were compared with a commercial  $\text{V}_2\text{O}_5/\text{WO}_3/\text{TiO}_2$  catalyst (CATCO), a standard material for use in diesel vehicles, as in references [4,5,23,29–31]. Before the catalytic runs, the catalysts were pre-treated in situ at  $350 \text{ }^\circ\text{C}$  for 2 h under a helium flow ( $30 \text{ cm}^3 \text{ min}^{-1}$ ). The reaction mixture typically consisted of 1000 ppm NO, 1000 ppm  $\text{NH}_3$ , and 2.5 vol.%  $\text{O}_2$  (balanced with He). The performance of a catalyst is generally a feature of its specific catalytic activity which, in turn, determines the required volume of catalyst. This is defined in terms of space velocity (S.V.), which is the exhaust gas volume per hour corrected to standard temperature and pressure divided by the catalyst volume. Typically, space velocities are  $30,000\text{--}100,000 \text{ h}^{-1}$  for diesel SCR and vary with the baseline emissions, required percentage of NOx reduction, and specific catalyst activity [32–34]. Thus, the total flow rate of the feed gas was  $150 \text{ mL min}^{-1}$ , Gas Hourly Space Velocity (GHSV)  $48,000 \text{ h}^{-1}$ .

It is important to highlight certain aspects, as that exhaust gases from diesel engines exhibit temperature, equivalence ratio and composition variations in response to load and speed regimes. Temperature and fuel/air equivalence ratios, for instance, are usually within the  $40 \text{ to } 560 \text{ }^\circ\text{C}$  and  $0.16 < \varphi < 0.78$  bands, respectively. As for nitrogen oxides emissions, typical diesel conditions range from 150 up to 1600 ppm.

In order to provide an adequate basis for catalyst efficiency comparisons with previously published data, a typical reaction mixture consisting of 1000 ppm NO, 1000 ppm  $\text{NH}_3$ , and 2.5 vol.%  $\text{O}_2$  in balance with He [4,5,28,33,34] was adopted.

The reaction temperature was scanned from  $100 \text{ to } 550 \text{ }^\circ\text{C}$ . Catalyst stability tests were performed at  $350 \text{ }^\circ\text{C}$  for 10 h by adding 50 ppm  $\text{SO}_2$  and 10 vol.%  $\text{H}_2\text{O}$  to the original feed. Meanwhile, the NO concentration of the inlet and outlet gases was measured using a NDIR multi gas analyzer (model GreenLine Eurothron) and  $\text{NH}_3$  was measured using an IQ350 ammonia analyzer (see apparatus diagram in Figure 1).

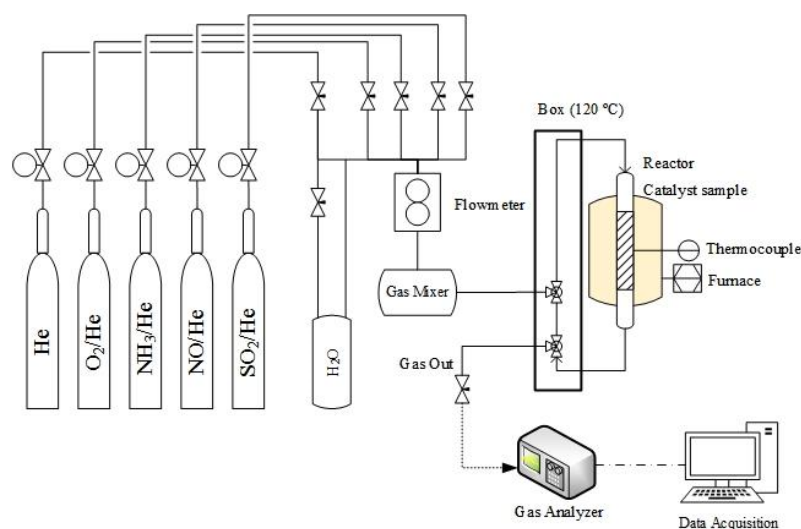


**Figure 1.** Apparatus diagram of the reaction system SCR.

The space velocity (S.V.) is defined as the volume of exhaust gas per hour corrected to standard temperature and pressure divided by the volume of the catalyst. Thus, the space velocity of a real catalyst in the exhaust of the diesel vehicle can refer to the wash coat volume of the SCR catalyst, which is 20% of the catalyst volume [29,33]. The typical

engine output data were converted to the typical space velocity referred to the active part of the catalyst as reported in the literature [4,5,23,29,31–33].

### 3. Results

#### 3.1. XRD and FTIR Structural Characterizations

To identify the structural characteristics of synthesized catalysts, XRD and FTIR techniques were used. XRD patterns shown in Figure 2a reveal peaks at  $2\theta = 9.87, 11.2, 17.35, 22.38, 22.76, 26.0, 28.0,$  and  $30.0^\circ$ , characteristic of natural clinoptilolite [33–36]. The low incidence of additional diffraction lines, characteristics of mordenite, and impurities (quartz and clays), confirms the zeolite composition supplied by Celta Brazil, consisting of 97% of clinoptilolite (CLIN) and only 3% of mordenite (MOR).

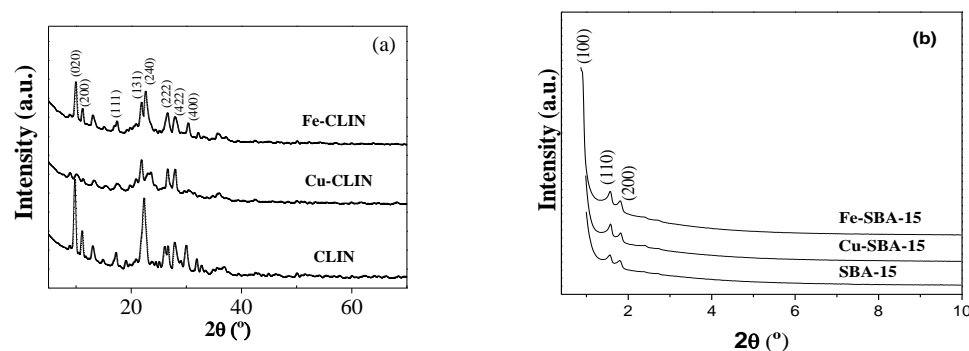


**Figure 2.** XRD patterns of the different catalysts based on CLIN (a) and SBA-15 (b).

There is no evidence of a change in the position of the main peaks of CLIN after the addition of Fe and Cu. However, the incorporation of transition metals by the ion-exchange method resulted in a slight decrease in the intensity of the main diffraction peaks, indicating the loss of the material's crystallinity. Peaks in the  $2\theta$  range between  $5$  and  $20^\circ$  were removed from the Cu-CLIN sample. This drastic change suggests significant destruction of the zeolite crystal structure. The characteristic reflection lines of Fe and Cu oxides were not detected, suggesting that the incorporation of metals by ion exchange was successful [37–39]. The low-angle XRD patterns of SBA-15, Cu-SBA-15, and Fe-SBA-15 catalysts are shown in Figure 2b. All the samples show diffraction peaks at  $2\theta = 0.96, 1.6,$  and  $1.8^\circ$ , indexed to the reflection planes (100), (110), and (200), respectively. These planes correspond to an ordered and well-defined hexagonal structure, characteristic of mesoporous materials of SBA-15 type [40,41].

No significant changes were observed on interplanar distance ( $d_{hkl}$ ) and on cell parameter ( $a_0$ ) of the hexagonal crystalline system of the support after the addition of the metals Fe and Cu (Table 1), indicating that the mesoporous structure of SBA-15 was preserved [42,43]. The impregnation of Fe caused an increase in the intensity of the diffraction peak intensity at  $0.94^\circ$ , characterizing the formation of a more ordered material with greater crystallinity. The absence of  $2\theta$  reflection lines between  $5$  and  $50^\circ$  (not shown) suggests that species formed by metals (cations or oxides of Fe and Cu) are highly dispersed on the surface, and they are not detected because their crystallite size is below the detection limit of XRD equipment [37–39].

The FTIR spectra of synthesized samples are shown in Figure 3a,b. There are two groups of vibration frequencies in all samples: (i) internal vibrations of T-O bond (considered insensitive to the structure) and (ii) vibrations of external bonds between tetrahedrons, due to the topology and the structural arrangement mode [24].

The FTIR spectrum of mesoporous silica (Figure 3a) shows absorption bands at  $800, 960,$  and  $1061\text{ cm}^{-1}$  and a shoulder at  $1193\text{ cm}^{-1}$ . The absorption band at  $1061\text{ cm}^{-1}$  is attributed to vibrations of asymmetric stretching of T-O connections (T = Si and Al), being sensitive to the amount of Si and Al in the network [33,35]. There is no evidence of band shifting with greater intensity in the FTIR spectra of Fe-SBA-15 and Cu-SBA-15

samples. This indicates the absence of Si and Al removal from SBA-15 network during metal impregnation. This result is in accordance with network parameters presented in Table 1, in which they show that the SBA-15 structure is maintained after Cu and Fe incorporation. The lower intensity band, located at  $960\text{ cm}^{-1}$ , has been associated with two types of vibrations: Si-OH symmetrical stretching vibrations or stretching vibrations of a  $[\text{SiO}_4]$  unit linked to heteroatoms [41,44,45]. The band at  $800\text{ cm}^{-1}$  and the shoulder at  $1193\text{ cm}^{-1}$  have been associated with O-T-O symmetrical stretching and T-O asymmetric stretching vibrations of F2 symmetry of  $\text{TO}_4$  tetrahedral group, respectively [44,45]. No significant change was observed in the frequency and intensity of these bands after the addition of Fe and Cu in the SBA-15 matrix.

**Table 1.** Textural and structural properties of pure SBA-15 and clinoptilolite supports and their respective catalysts.

Catalysts	Cu Content (wt.%)	Fe Content (wt.%)	$S_{\text{BET}}$ ( $\text{m}^2\text{ g}^{-1}$ )	$V_{\text{p}}$ ( $\text{cm}^3\text{ g}^{-1}$ )	$D_{\text{p}}$ (nm)	$d_{\text{hkl}}$ (nm)	$a_0$ (nm)
CATCO	-	-	44.9	0.24	20.3	-	-
SBA-15	-	-	709	1.02	6.8	8.8	10.2
Cu-SBA-15	1.6	-	638	0.95	6.7	8.9	10.3
Fe-SBA-15	-	2.0	671	0.97	6.7	8.9	10.3
CLIN	-	1.4	33.2	0.14	24.3	-	-
Cu-CLIN	1.7	1.4	33.8	0.14	23.8	-	-
Fe-CLIN	-	1.7	150	0.21	19.6	-	-

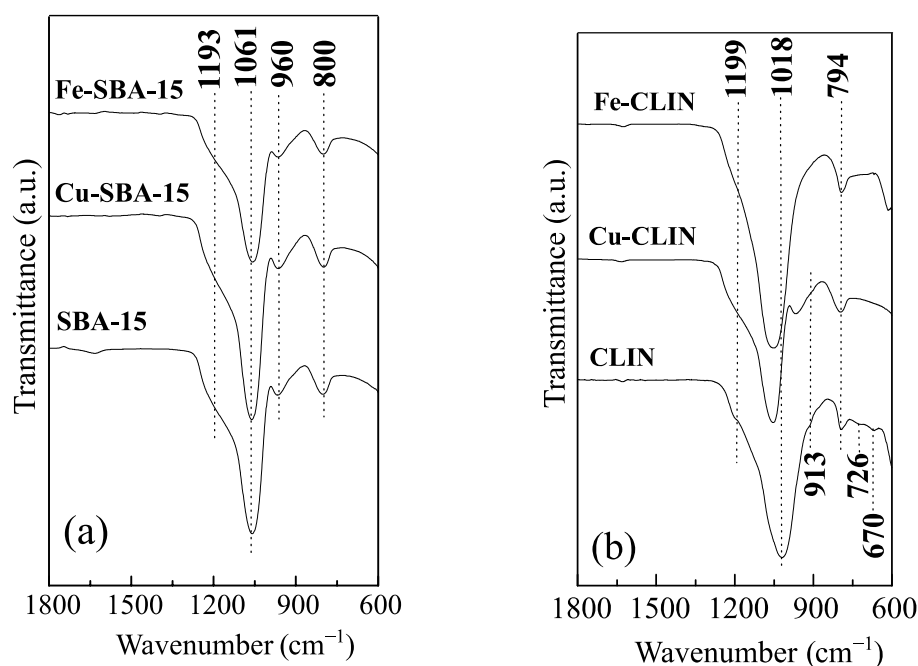


**Figure 3.** FTIR spectra of the catalysts based on SBA-15 (a) and CLIN (b).

The FTIR spectrum of clinoptilolite (Figure 3b) indicates absorption bands at  $670$ ,  $726$ ,  $794$ , and  $1018\text{ cm}^{-1}$  and shoulders at  $913\text{ cm}^{-1}$  and  $1199\text{ cm}^{-1}$ . The assignments of the absorption bands at  $794$ ,  $913$ ,  $1018$  and  $1199\text{ cm}^{-1}$  are similar to those presented for bands at  $800$ ,  $960$ ,  $1061$  and  $1193\text{ cm}^{-1}$  of samples based on SBA-15. The low-intensity bands located at  $670$  and  $726\text{ cm}^{-1}$  have been assigned to asymmetric stretching vibrations of  $\text{TO}_4$  tetrahedral group. The incorporation of Cu in the zeolite matrix causes suppression of the low-intensity bands ( $670$  and  $726\text{ cm}^{-1}$ ) and an increase in the intensity of the band at  $794\text{ cm}^{-1}$ . In addition, the shoulder at  $913\text{ cm}^{-1}$  is shifted to the high-frequency region, appearing as a more defined band with greater intensity at  $967\text{ cm}^{-1}$ , indicating

the existence of metal ions in CLIN network,  $M\text{-}[\text{SiO}_4]$  [45,46]. Likewise, the  $1018\text{ cm}^{-1}$  band is moved  $39\text{ cm}^{-1}$  to a higher frequency region ( $1057\text{ cm}^{-1}$ ). This suggests Si and Al removal from the CLIN network, resulting in a partial structural change, accompanied by dealumination [47].

This fact was evidenced by the X-ray pattern of the Cu-CLI sample (Figure 1a) which shows a significant destruction of the zeolite structure. The incorporation of Fe caused effects similar to those reported for the sample promoted with Cu. However, the  $913\text{ cm}^{-1}$  band cannot be identified in the Fe-CLIN sample spectrum, due to the widening of the vibration band at  $1052\text{ cm}^{-1}$ , which appears in a region between  $857$  and  $1296\text{ cm}^{-1}$ . Similarly, the display of the band at  $1199\text{ cm}^{-1}$  was also compromised, appearing only as a poorly defined shoulder at  $1217\text{ cm}^{-1}$ .

### 3.2. Textural Properties and Acidity

Textural characteristics of clinoptilolite-based catalysts are presented in Table 1, as well as the Metal content (wt.%). There are no significant changes in the  $S_{\text{BET}}$ ,  $V_p$  and  $D_p$  values after the incorporation of Cu in the clinoptilolite matrix. On the other hand, a specific surface area of  $150\text{ m}^2\text{ g}^{-1}$  was observed for the Fe-CLIN system, considerably larger than the non-promoted zeolite area ( $33.2\text{ m}^2\text{ g}^{-1}$ ). This increase has been assigned to the formation of species such as: (i) non-crystalline Fe, (ii) binuclear and oligonuclear Fe complexes, and (iii) FeOx type Fe oxides. These species have been located at cationic positions of zeolite channels, in extra-network positions and on the surface of zeolite crystals, respectively [47]. In the case of SBA-15 samples,  $d_{\text{hkl}}$  represents the interplanar distance. The presented results demonstrated that there is a structural uniformity between the catalysts promoted with metals and the support. This indicates that a hexagonal structure was preserved even after the impregnation of metals in the SBA-15 matrix. Therefore, there was no significant loss of crystallinity in relation to the starting material [38,43,48].

The crystallinity decreases of the Fe-CLIN sample (3D crystalline structure), evidenced by the X-ray diffractogram (Figure 2a), demonstrate that the presence of a slightly amorphous phase may be desirable, since it results in the increase in the specific surface area. Adsorption isotherms for all samples are of type II, characteristic of mesoporous surfaces, and these are shown in Figure 4a [43]. There is no similarity between hysteresis identified in Figure 4a and IUPAC classification (H1, H2, H3 and H4). Hysteresis loops of samples based on clinoptilolite close at a relative pressure between 0.6–0.8, while the IUPAC desorption isotherms close between 0.4–0.5 and can continue at pressures near zero. Similar behaviors were obtained in another work [49], which assigned this modification to a physical alteration in the adsorbent known as irreversible swelling of non-rigid pores. Due to the zeolite compound nature (consisting of zeolite crystals and amorphous agglutinative), there is a high probability of this phenomenon occurring during the adsorption–desorption process [36,48].

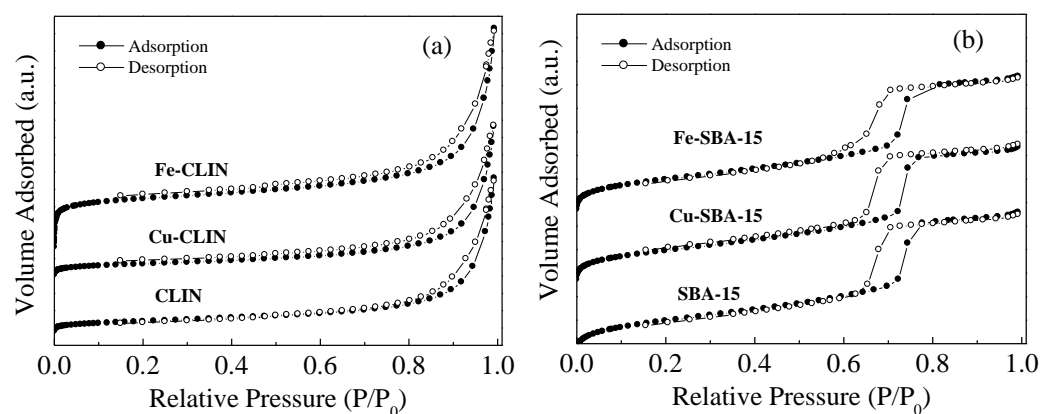


**Figure 4.**  $\text{N}_2$  adsorption–desorption isotherms at  $-196\text{ }^\circ\text{C}$  of the catalysts based on CLIN (a) and SBA-15 (b).

The N<sub>2</sub> adsorption–desorption isotherms shown in Figure 4b are classified as type IV isotherms and with type H1 hysteresis (IUPAC). These are typical for cylindrical mesoporous materials ordered with a hexagonal 2D structure [17,49]. The presence of an accentuated step at relatively high pressure ( $P/P_0 = 0.8$ ) has been assigned to the capillary condensation of N<sub>2</sub> inside the mesopores [17].

As shown in Table 1, the specific surface area and the pore size of the SBA-15 support were reduced to some extent after the addition of the active metals (Cu and Fe). This has been assigned to the partial blockage of SBA-15 mesoporous channels by species formed during calcination, such as particles or metal oxides [42,50]. Despite this, wet impregnation can be considered efficient for metal incorporation into mesoporous materials, since it does not interfere with the ordered pore structure of the SBA-15 support.

Figure 5 shows pyridine-adsorbed IR spectra at 25 and 100 °C. The band at 1440 cm<sup>-1</sup> has been associated with the adsorption of pyridine at Lewis acid sites (L-Py). No band was observed in the region between 1540 and 1548 cm<sup>-1</sup>, characteristic of pyridine adsorbed on Brønsted acid sites (B-Py). The presence of bands at 1484 and 1595 cm<sup>-1</sup> has been attributed to the collective contributions of L-Py and B-Py and hydrogen-bound pyridine (hb-Py), respectively [49].

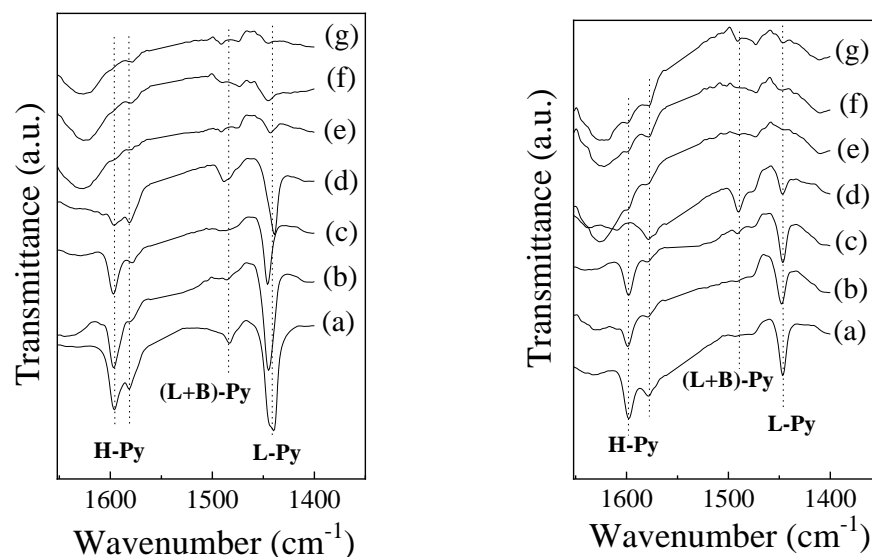


**Figure 5.** FT-IR spectra of adsorbed pyridine at 25 °C (left) and 100 °C (right) in (a) SBA-15, (b) Cu-SBA-15, (c) Fe-SBA-15, (d) CATCO, (e) CLIN, (f) Cu-CLIN and (g) Fe-CLIN catalysts.

As observed in Figure 5 (left plot), there is a predominance of L-Py adsorption bands on the support and catalysts based on SBA-15. On the other hand, these adsorption bands present low intensity in metal/CLIN catalysts, indicating that these samples have low acidity. The L-Py band area decreases with increasing adsorption temperature (Figure 5 (right plot)), indicating weak adsorption of pyridine with the Lewis acid sites.

A considerable increase in the concentration of Lewis acid sites was observed (Table 2) after the incorporation of Fe and Cu in the SBA-15 support. A similar effect was observed in catalysts supported by CLIN. This effect has been related to the presence of superficial copper and iron species, which can bind pyridine molecules in a coordinated way [49].

**Table 2.** Acid sites of the materials.

Supports and Catalysts	<sup>a</sup> Total Acid Sites Amount ( $\mu\text{mol Py g}^{-1}$ )
CATCO	1.43
	0.91
SBA-15	1.61
	0.37

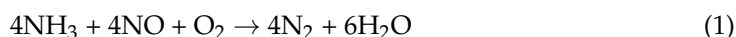
Table 2. Cont.

Supports and Catalysts	<sup>a</sup> Total Acid Sites Amount ( $\mu\text{mol Py g}^{-1}$ )
Cu-SBA-15	5.58
	1.37
Fe-SBA-15	3.46
	0.23
CLIN	0.29
	0.09
Cu-CLIN	1.71
	0.72
Fe-CLIN	0.88
	0.82

<sup>a</sup> Measured by FT-IR spectra of adsorbed pyridine at 25 °C (the first number) and 100 °C (the second number).

### 3.3. Activity Tests

The selective catalytic reduction of NO in the presence of NH<sub>3</sub> and an excess of O<sub>2</sub> can be represented according to the reaction described by Equation (1).



The conversion efficiencies of NO as a function of temperature over the natural clinoptilolite (CLIN), ordered mesoporous silica SBA-15 and metal-doped materials (Cu-CLIN, Fe-CLIN, Cu-SBA-15, Fe-SBA-15) are compared in Figure 6. The activity of a commercial V<sub>2</sub>O<sub>5</sub>/WO<sub>3</sub>/TiO<sub>2</sub> SCR catalyst (CATCO) for mobility diesel engines is also shown as a reference. As expected, due to the lack of acid sites and redox centers, SBA-15 showed insignificant NH<sub>3</sub>-SCR activity, exhibiting NO conversion values lower than 11% in the whole reaction temperature range. At low temperatures, the natural clinoptilolite showed low activity, attaining a maximum NO conversion value of about 20% at 350 °C. On the other hand, a NO conversion higher than 80% was verified at a reaction temperature of 500 °C. Those catalytic results can be explained by the presence of iron and other metal species in the chemical composition of the used natural zeolite. The NH<sub>3</sub>-SCR activity of the natural clinoptilolite and ordered mesoporous silica SBA-15 notably increases when Cu and Fe were incorporated. At low and medium operating temperatures (100–300 °C), all samples containing Cu showed better NO conversion values when compared with Fe-doped samples. Above 300 °C, clinoptilolite catalysts were more active than those based on SBA-15. Up to temperatures around 350 °C, the NO conversion rate over doped clinoptilolite catalysts has an increasing behavior. For these catalysts, it is proposed that NH<sub>3</sub> adsorption occurs on the acid sites of these materials. This fact has been investigated by several authors [24,29,41]. As a matter of fact, SCR reaction occurs when NO or NO<sub>2</sub> reacts with the adsorbed NH<sub>3</sub> [18,24,39,41,49,51].

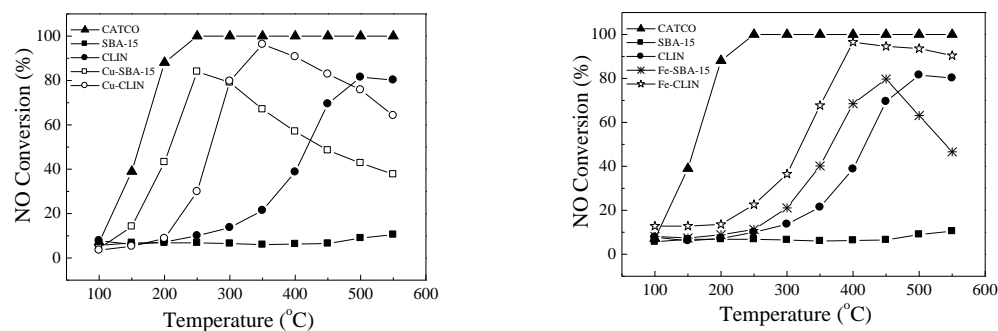


**Figure 6.** SCR performance of NO conversion with NH<sub>3</sub> over various catalysts. Reaction conditions: [NH<sub>3</sub>] = [NO] = 1000 ppm, [O<sub>2</sub>] = 2.5 vol.%, total flow rate = 150 mL.min<sup>-1</sup> and GHSV = 48,000 h<sup>-1</sup>. Reaction conditions to copper (left) and iron catalysts (right).

According to Figure 6 and Table 2, maximum conversions of about 96% were observed for Cu-CLIN and Fe-CLIN at 350 °C and 400 °C, respectively. At higher temperatures, there is a decrease in the NO conversion rate over both samples. However, the decrease is more pronounced for the Cu-doped clinoptilolite catalyst. A net activity decrease at high reaction temperatures is commonly verified for NH<sub>3</sub>-SCR catalysts due to an intense NH<sub>3</sub> oxidation rate [4,5,52]. The unselective reaction that represents the catalytic oxidation of NH<sub>3</sub> is described by Equation (2).



According to Figure 6 and Table 2, maximum conversions of about 84% and 80% were observed for Cu-SBA-15 and Fe-SBA-15 at 250 °C and 450 °C, respectively. Above such temperatures, a decreasing NO conversion rate is verified for both samples.

In summary, all the findings reveal effective NO<sub>x</sub> removal efficiencies and considerable operating temperature windows using natural zeolite catalysts based on both copper and iron. On the other hand, for SBA-15 support Cu doped samples performed better at 250 °C, whereas Fe-doped samples exhibited superior efficiencies at higher temperatures. Optimal values of the Si/Al ratio were found to play a crucial role and further studies on the variation of this rate and adsorbed monodentate nitrates are required to obtain a fundamental understanding of their impact on low-temperature SCR activity. Such aspects are fundamental for catalyst-quality analysis, since a wider temperature window and ignition below 350 °C with good hydrothermal stability are requirements that must be simultaneously achieved [53]. Figure 7 shows the evolution of the stability of catalysts during the SCR of NO with NH<sub>3</sub> in the presence of SO<sub>2</sub> and H<sub>2</sub>O at 350 °C. In other words, this study investigates the aging of the catalyst in the presence of SO<sub>2</sub> and water vapor (% H<sub>2</sub>O *v/v*). A very promising NO conversion efficiency at 350 °C for Fe-CLIN catalysts (above 85%) was observed (Figure 7a). This behavior was also reported by literature [29,54] for CATCO (approximately 91%) in the presence of water. However, in the presence of SO<sub>2</sub> both FeMORD and CATCO catalysts show a NO conversion efficiency above 91%. On the contrary, the FeZSM5 catalyst reveals a considerable decrease in the NO conversion efficiency when introducing SO<sub>2</sub> in the feed. Furthermore, no substantial deactivation was observed after 10 h of reaction.

In general, it is observed that there was a reduction between 2 and 14% of the catalytic activity of the catalysts tested in the presence of SO<sub>2</sub>. However, this effect is less pronounced in catalysts based on SBA-15 (2–5%), exhibiting greater stability of mesoporous solids in the presence of sulfur dioxide. SO<sub>2</sub> adsorption is competitive with NH<sub>3</sub> adsorption at Lewis acid sites and occurs rapidly and irreversibly at low temperatures. Sulfur dioxide reacts with surface ions producing sulfite and sulfate species at temperatures between 200 and 350 °C. Above 350 °C in the presence of oxygen, only sulfate species are formed on the surface, whereas sulfur trioxide (SO<sub>3</sub>) is adsorbed at higher temperatures, which can lead to a reduction in the activity of catalysts in the presence of SO<sub>2</sub> [53–55].

The introduction of 10% of water vapor into the reaction did not show any deactivation in the Fe-zeolite catalysts, presenting considerable selectivity of nitrogen (see Figure 7c). Water adsorbs more easily than ammonia on the surface of catalysts, although it does not completely inhibit its adsorption on the catalyst. However, work on stability with water shows that the catalytic inhibition caused by the presence of water in the gaseous stream is more pronounced at temperatures below 400 °C, mainly due to the adsorption of H<sub>2</sub>O at redox sites [56]. These explanations are consistent with the results obtained in the present work, since the catalysts, doped with iron, which have a conversion temperature above 400 °C are much more stable in their conversion percentages in the presence of water than the other catalysts doped with copper, which have a lower conversion temperature.

The presence of H<sub>2</sub>O and SO<sub>2</sub> in the same gaseous stream has an even more pronounced effect than those observed in isolated tests. There is a reduction from 7.9 to 29.6% in the conversion of catalysts in the presence of these two contaminants. Obviously, the combined effects of each poison on the catalyst assume a greater drop in conversion on these tests [57]. The commercial catalyst has been presented [23,29] and no apprecia-

ble deactivation after 10 h of reaction was observed in the presence of H<sub>2</sub>O vapor and sulfur dioxide.

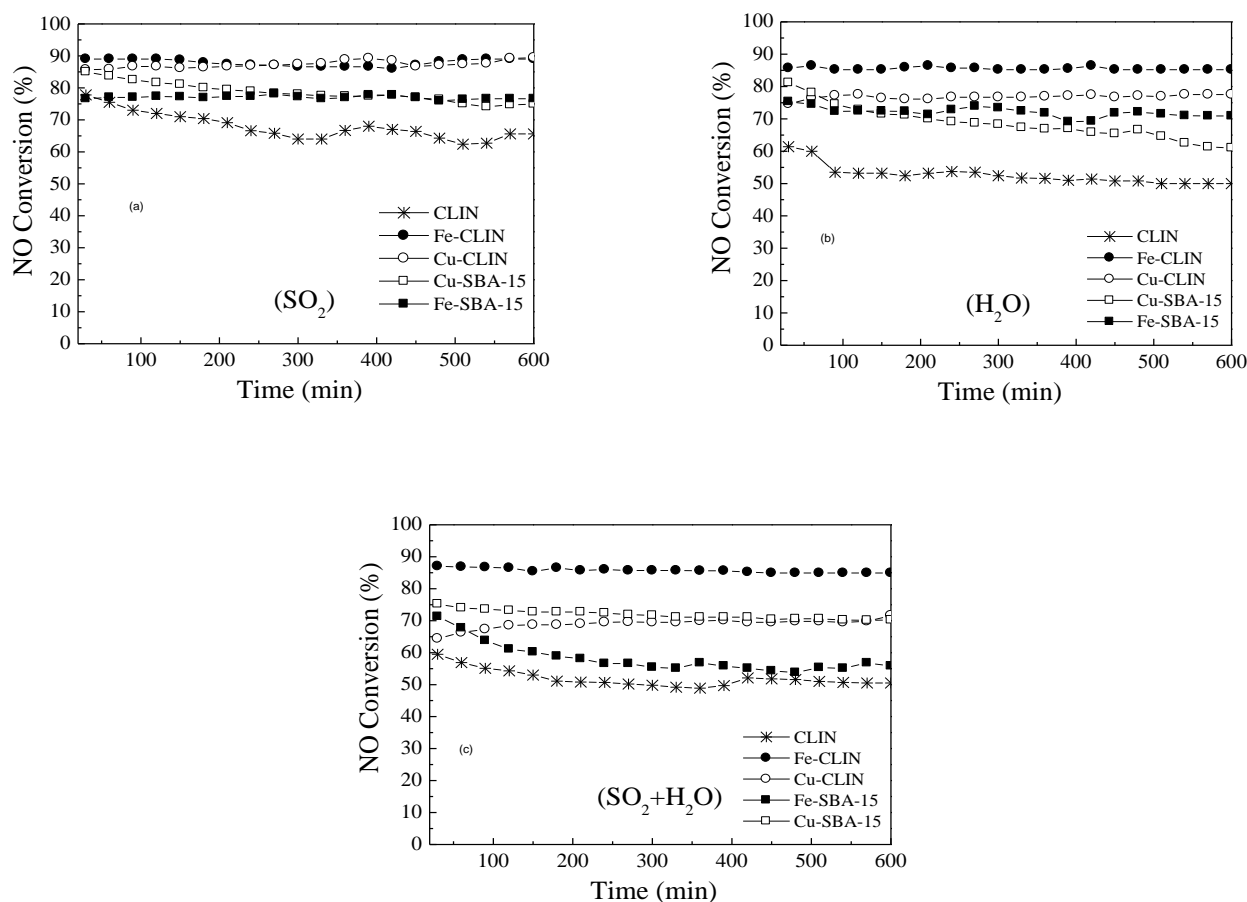


**Figure 7.** Evolution on stability of catalysts during the SCR of NO with NH<sub>3</sub> at 350 °C with total flow rate = 150 mL·min<sup>-1</sup> and GHSV = 48,000 h<sup>-1</sup>. Reaction conditions: [NH<sub>3</sub>] = [NO] = 1000 ppm, [O<sub>2</sub>] = 2.5 vol.%, [SO<sub>2</sub>] = 50 ppm (a), [H<sub>2</sub>O] = 10 vol.% (b) and [SO<sub>2</sub>] = 50 ppm + [H<sub>2</sub>O] = 10 vol.% (c).

Table 3 summarizes the experimental results of the tested catalysts in standard, water vapor, and SO<sub>2</sub> conditions. The stability CATCO catalyst data were presented mainly for comparison since they have already been previously presented in other works cited above.

**Table 3.** Catalysis data.

Catalysts	Maximum Temperature Conversion (°C)	% Maximum Conversion	Stability		
			SO <sub>2</sub>	H <sub>2</sub> O	SO <sub>2</sub> + H <sub>2</sub> O
			<sup>a</sup> MC (%)	<sup>a</sup> MC (%)	<sup>a</sup> MC (%)
CATCO	250	100	-	-	-
SBA-15	550	10.5	-	-	-
Cu-SBA-15	250	84.1	78.5	68.7	58.2
Fe-SBA-15	450	79.7	77.1	72.1	71.8
CLIN	500	81.5	67.9	52.7	51.9
Cu-CLIN	350	96.3	87.4	76.8	69.1
Fe-CLIN	400	96.5	87.9	85.7	85.4

<sup>a</sup> Legend: MC = % media conversion in 10 h.

As shown in Table 3, the iron-exchanged CLIN has higher catalytic activity in all test conditions than the natural zeolite. In general, the conventional ion-exchange method

produces preferably large iron oxide clusters as well as a small amount of isolated Fe sites. Accordingly, in cluster-free samples, isolated  $\text{Fe}^{3+}$  ions are partially reduced under steady-state SCR conditions. Thus, it is possible that among the isolated Fe species, the reducible  $\text{Fe}^{3+}$  ions might be the only ones that have an active role in the SCR reaction. So, it is generally agreed that monomeric Fe species are more active in this reaction [57,58]. As mentioned, commercial vanadia-based SCR catalysts typically contain titania as support, vanadia as active component, and molybdenum oxide as structural and chemical promoters (i.e.,  $\text{V}_2\text{O}_5\text{-WO}_3/\text{TiO}_2$ ). The anatase  $\text{TiO}_2$  with high surface area possesses high acidity and high resistance against sulfur poisoning, whereas the well-dispersed vanadium species, below a monolayer coverage, have been reported as the redox-active component in  $\text{NO}_x$  reduction. The standard SCR performance of the vanadia-SCR catalyst showed the highest  $\text{NO}_x$  conversion, indicating that, also in this case, V sites are the main active species in this reaction in comparison with other catalysts in this study.

#### 4. Discussion

A comparison between the results obtained in the current work and the available literature is provided in Table 4. NO conversions were determined from Cu-SSZ-13 catalysts synthesized with three Si/Al ratios of 6, 15, and 30 [58]. In comparison, the authors observed that the Cu-SSZ-13 with Si/Al = 15 exhibits better higher  $\text{NH}_3$ -SCR catalytic activity and much better resistance to hydrothermal aging. Based on XRD, BET, EPR and  $\text{H}_2$ -TPR results, they suggest that when the Si/Al ratio is at a moderate range,  $\text{Cu}^{2+}$  ions are well-preserved and the zeolite framework is stable enough to sustain the dealumination during the hydrothermal treatment. In this way, a suitable Si/Al ratio was very important to the de  $\text{NO}_x$  performance and hydrothermal stability of the Cu-SSZ-13 catalyst according to those authors. Although NO conversions over 95% have been observed for both Si/Al-6 and Si/Al-15 catalysts from 225 to 550 °C, the Cu-SSZ-13 with Si/Al = 15 is much more resistant to hydrothermal aging, which makes it a better candidate for diesel exhaust purification.

It was shown [57] that the Cu-SSZ-13 zeolite–metal oxide hybrid catalysts, prepared by the sol-dispersion method, exhibit an excellent  $\text{NH}_3$ -SCR reactivity and enhanced tolerance towards  $\text{SO}_2$ -poisoning when compared to the Cu-SSZ-13 zeolite. These authors pointed out that metal oxide may serve as a sacrificial component that undergoes preferential  $\text{SO}_2$ -poisoning, thereby improving  $\text{SO}_2$ -tolerance.

According to the literature [58,59], Fe/SSZ-13 catalysts synthesized using a traditional aqueous solution ion-exchange method under a protecting atmosphere of  $\text{N}_2$  are also active in  $\text{NH}_3$ -SCR. A maximum NO conversion of about 88.0% can be observed for a fresh sample (Fe/SSZ-13 catalyst without hydrothermal aging) at temperatures close to 330 °C, under dry conditions. However, SCR becomes substantially less selective above 300 °C, demonstrating more extensive non-selective  $\text{NH}_3$  oxidation. In the presence of  $\text{H}_2\text{O}$ , high and stable SCR selectivities of about 90% were maintained in a wide temperature range from 350 to 550 °C. Above 400 °C, even with extremely severe hydrothermal aging, Fe/SSZ-13 maintains structural integrity and much of the SCR activities. In line with what was observed for the Fe-CLIN catalyst studied in the present work, the Fe/SSZ-13 catalysts previously synthesized [58] also showed a lack of low-temperature activity as compared with Cu-doped samples. The iron catalyst has maintained its structural integrity and much of the SCR activities, especially that  $\text{Fe}^{3+}$  at different sites were also found to present different hydrothermal stability, and those in ion-exchanged sites were more stable than those in residual protonic sites [59,60].

In the current work, abundant support materials were associated to restrict levels of catalyst loading in order to explore affordable  $\text{NO}_x$  mitigation material alternatives. The results are in agreement with the literature and clinoptilolite with incorporated Cu and Fe exhibited catalytic efficiencies above 96% (see Figure 6). With regards to durability, the Fe doped catalyst showed very high stability in the presence of  $\text{SO}_2$  and water at 350 °C and after 10 h of reaction. Prospects of this research may include engine dynamometric tests

in order to better explore the attractivity of the Fe-CLIN catalysts from the prospects of performance and end-product cost.

Table 4 summarizes some data from research works related to the use of Fe- and Cu-doped catalysts in the NH<sub>3</sub>-SCR of NO<sub>x</sub>. Authors reported [30] the test of Fe-BEA and Cu-BEA catalysts in the SCR system. The NO<sub>x</sub> conversion of these metal-zeolite catalysts remained greater than 80% in the temperature range of 300 and 450 °C. But, compared to the Fe/BEA catalyst, the Cu/BEA catalyst in the urea-SCR after-treatment systems exhibited higher NO and NO<sub>2</sub> conversion efficiencies while maintaining a lower amount of N<sub>2</sub>O formation in this temperature range. In general, the ammonia storage capability of Cu/zeolite was higher than that of Fe/zeolite.

The difference in the NO conversion between catalyst-based ZSM5 (or MFI) and Mordenite can be related to their Si/Al ratio, channel system, and framework type. The ZSM5 zeolite has a three-dimensional channel system and pore openings of 5.3 × 5.6 Å and 5.1 × 5.5 Å. However, iron sites in zeolites are accessible to form NO complexes, as mentioned in natural CLIN catalyst from this study. Nevertheless, the natural Mordenite has a 1-dimensional channel system framework type, which makes this zeolite quite vulnerable, since blocking of the pore mouths suffices to prevent gas-phase molecules from reaching active sites inside the channels. Similar results of NO conversion efficiency (about 95%) were obtained in the standard test for Metals-ZSM5 [23,29] and Metals-CLIN in a temperature range of 350–400 °C.

In general, for the zeolites catalyst, the reducibility of copper(II) is a function of both the nature of the support and the dispersion degree of the active phase. The presence of strong acidity in the catalysts enhanced the selectivity to N<sub>2</sub>, as well as the Fe-zeolite.

**Table 4.** Summary of NH<sub>3</sub>-SCR of NO<sub>x</sub> from literature data \*.

Catalyst	% Metal Loading (wt.%)	Maximum Temperature Conversion (°C)	Maximum NO Abatement %	Reference
Cu-SBA-15	1.6	250	84.1	This work
Fe-SBA-15	2.0	450	79.7	
Cu-CLIN	1.7	350	96.3	
Fe-CLIN	1.7	400	96.5	
Fe-ZSM5	2.0	350	95.0	[23]
Cu-ZSM5	2.0	350	98.1	[29]
Cu-MORD	4.0	350	100	
Fe-MORD	4.0	350	100	
Cu/SSZ-13	2.8	250–350	99.0	[57]
Cu/SSZ-13	2.0	150–600	73.0	[26]
Fe/SSZ-13	1.37	330	88.0	[61]
Cu/BEA	2.0	300	99.0	[27]
Fe/BEA	2.0	400	99.0	
CuPPH(Cu3i)	3.0	400	95.7	[31]

\* Standard test data for each work.

## 5. Conclusions

Natural clinoptilolite (CLIN) from Slovakia is active in the SCR of NO by NH<sub>3</sub> in an excess of O<sub>2</sub>, exhibiting a maximum NO conversion value of 81.5% at 500 °C and very low activity in the temperature range of 100–350 °C. The incorporation of Fe and Cu transition metals into the natural zeolite structure was able to increase the catalytic activity even at low temperatures. Both Cu- and Fe-doped samples showed maximum conversions of about 96% at 350 °C and 400 °C, respectively. In addition, the Fe-CLIN catalyst showed very high stability in the presence of O<sub>2</sub>, SO<sub>2</sub> and water steam at 350 °C and after 10 h of reaction. Catalysts capable of operating at low and medium temperature conditions are especially necessary when the reaction device is installed downstream of the flue gas.

This strategy is an effective way to prevent catalyst poisoning, but it requires temperatures below 300 °C [31]. On the other hand, catalysts more active and stable at high temperatures are suitable for diesel engine exhaust after treatment. The Cu- and Fe-doped catalysts based on SBA-15 also have activity for the SCR of NO by NH<sub>3</sub> in an excess of O<sub>2</sub>. However, the NO conversion rates in these samples are lower than those observed in doped clinoptilolite catalysts. Maximum conversions of about 84% and 80% were verified for Cu-SBA-15 and Fe-SBA-15, at 250 °C and 450 °C, respectively.

**Author Contributions:** A.P.M.P.A. and R.d.S.A.: catalysts preparation and experimental setup, J.C.S.d.A., R.K.C.d.L. and E.R.-C.: characterization analysis and writing—original draft, A.V.B., M.E.V.d.S. and P.A.C.R. review and editing, M.L.M.d.O.: data validation, review and supervision. All authors have read and agreed to the published version of the manuscript.

**Funding:** This study was financed in part by the Coordenação de Aperfeiçoamento de Pessoal de Nível Superior—Brasil (CAPES)—Finance Code 001 and by the Conselho Nacional de Desenvolvimento Científico e Tecnológico—Brasil (CNPq), Grant No. 303585/2022-6. The Celta Brazil Ltda. providing the natural zeolite is gratefully acknowledged. E.R.C. thanks to project PID2021-126235OB-C32 of Ministerio de Ciencia e Innovación of Spain/AEI and FEDER funds.

**Institutional Review Board Statement:** Not applicable.

**Informed Consent Statement:** Not applicable.

**Data Availability Statement:** The data presented in this study are available on request from the corresponding author. The data are not publicly available due to institutional restrictions.

**Acknowledgments:** The natural zeolite provided by Celta Brazil Ltda. is gratefully acknowledged.

**Conflicts of Interest:** The authors declare no conflict of interest.

## References

1. Hagan, R.; Markey, E.; Clancy, J.; Keating, M.; Donnelly, A.; O'Connor, D.J.; Morrison McGillicuddy, E.J. Non-Road Mobile Machinery Emissions and Regulations: A Review. *Air* **2023**, *1*, 14–36. [[CrossRef](#)]
2. Policarpo, N.A.; Silva, C.; Lopes, T.F.A.; Araújo, R.S.; Cavalcante, F.S.A.; Pitombo, C.S.; Oliveira, M.L.M. Road vehicle emission inventory of a Brazilian metropolitan area and insights for other emerging economies. *Transp. Res. Part D Transp. Environ.* **2018**, *58*, 172–185. [[CrossRef](#)]
3. Saboori, B.; Sapri, M.; Baba, M. Economic growth, energy consumption and CO<sub>2</sub> emissions in OECD (Organization for Economic Co-operation and Development)'s transport sector: A fully modified bi-directional relationship approach. *Energy* **2014**, *66*, 150–161. [[CrossRef](#)]
4. Moreno-Tost, R.; Santamaría-González, J.; Rodríguez-Castellón, E.; Jiménez-López, A.; Autié, M.A.; González, E.; Glacial, M.C.; De las Pozas, C. Selective catalytic reduction of nitric oxide by ammonia over Cu-exchanged Cuban natural zeolites. *Appl. Catal. B Environ.* **2004**, *50*, 279–288. [[CrossRef](#)]
5. Moreno-Tost, R.; Santamaría-González, J.; Rodríguez-Castellón, E.; Jiménez-López, A.; Autié, M.A.; Glacial, M.C.; Castro, G.A.; Guerra, M. Selective Catalytic Reduction of Nitric Oxide by Ammonia over Ag and Zn-Exchanged Cuban Natural Zeolites. *Z. Für Anorg. Und Allg. Chem.* **2005**, *631*, 2253–2257. [[CrossRef](#)]
6. Sounak, R.; Hegde, M.S.; Giridhar, M. Catalysis for NOx abatement. *Appl. Energy* **2009**, *86*, 2283–2297. [[CrossRef](#)]
7. Kwon, D.W.; Nam, K.B.; Hong, S.C. Influence of tungsten on the activity of a Mn/Ce/W/Ti catalyst for the selective catalytic reduction of NO with NH<sub>3</sub> at low temperatures. *Appl. Catal. A Gen.* **2015**, *497*, 160–166. [[CrossRef](#)]
8. Oliveira Santos, V.; Costa Rocha, P.A.; Scott, J.; Van Griensven Thé, J.; Gharabaghi, B. Spatiotemporal Air Pollution Forecasting in Houston-TX: A Case Study for Ozone Using Deep Graph Neural Networks. *Atmosphere* **2023**, *14*, 308. [[CrossRef](#)]
9. Li, X.; Li, X.; Chen, J.; Li, J.; Hao, J. An efficient novel regeneration method for Ca-poisoning V<sub>2</sub>O<sub>5</sub>-WO<sub>3</sub>/TiO<sub>2</sub> catalyst. *Catal. Commun.* **2016**, *87*, 45–48. [[CrossRef](#)]
10. Shi, J.; Zhang, Z.; Chen, M.; Zhang, Z.; Shangguan, W. Promotion effect of tungsten and iron co-addition on the catalytic performance of MnO<sub>x</sub>/TiO<sub>2</sub> for NH<sub>3</sub>-SCR of NOx. *Fuel* **2017**, *210*, 783–789. [[CrossRef](#)]
11. Long, R.Q.; Yang, R.T. Selective Catalytic Reduction of NO with Ammonia over Fe<sup>3+</sup>-Exchanged Mordenite (Fe-MOR): Catalytic Performance, Characterization, and Mechanistic Study. *J. Catal.* **2002**, *207*, 274–285. [[CrossRef](#)]
12. Kim, M.H.; Nam, I.S.; Kim, Y.G. Water tolerance of mordenite-type zeolite catalysts for selective reduction of nitric oxide by hydrocarbons. *Appl. Catal. B Environ.* **1997**, *12*, 125–145. [[CrossRef](#)]
13. Brandin, J.G.M.; Andersson, L.A.H.; Odenbrand, C.U.I. Catalytic reduction of nitrogen oxides on mordenite some aspect on the mechanism. *Catal. Today* **1989**, *4*, 187–203. [[CrossRef](#)]

14. Corma, A.; Fornes, V.; Palomares, E. Selective catalytic reduction of NO<sub>x</sub> on Cu-beta zeolites. *Appl. Catal. B Environ.* **1997**, *11*, 233–242. [[CrossRef](#)]
15. Rahkamaa-Tolonen, K.; Maunula, T.; Lomma, M.; Huuhtanen, M.; Keiski, R.L. The effect of NO<sub>2</sub> on the activity of fresh and aged zeolite catalysts in the NH<sub>3</sub>-SCR reaction. *Catal. Today* **2005**, *100*, 217–222. [[CrossRef](#)]
16. Liang, X.; Li, J.; Lin, Q.; Sun, K. Synthesis and characterization of mesoporous Mn/Al-SBA-15 and its catalytic activity for NO reduction with ammonia. *Catal. Commun.* **2007**, *8*, 1901–1904. [[CrossRef](#)]
17. Zhang, H.; Tang, C.; Sun, C.; Qi, L.; Gao, F.; Dong, L.; Chen, Y. Direct synthesis, characterization and catalytic performance of bimetallic Fe–Mo-SBA-15 materials in selective catalytic reduction of NO with NH<sub>3</sub>. *Microporous Mesoporous Mater* **2012**, *151*, 44–55. [[CrossRef](#)]
18. Tu, C.H.; Wang, A.Q.; Zheng, M.Y.; Wang, X.D.; Zhang, T. Factors influencing the catalytic activity of SBA-15-supported copper nanoparticles in CO oxidation. *J. Appl. Catal. A Gen.* **2006**, *297*, 40–47. [[CrossRef](#)]
19. Chmielarz, L.; Kuśtrowski, P.; Dziembaj, R.; Cool, P.; Vansant, E.F. Catalytic performance of various mesoporous silicas modified with copper or iron oxides introduced by different ways in the selective reduction of NO by ammonia. *Appl. Catal. B Environ.* **2006**, *62*, 369–380. [[CrossRef](#)]
20. Iznaga, I.R.; Petranovskii, V.; Fuentes, G.R.; Mendoza, C.; Aguilar, A.B. Exchange and reduction of Cu<sup>2+</sup> ions in clinoptilolite. *J. Colloid Interface Sci.* **2007**, *316*, 877–886. [[CrossRef](#)]
21. Bello, E.; Ferri, P.; Nero, M.; Willhammar, T.; Millet, I.; Schütze, F.W.; Tendeloo, L.W.; Vennestrøm, P.N.R.; Boronat, M.; Corma, A.; et al. NH<sub>3</sub>-SCR catalysts for heavy-duty diesel vehicles: Preparation of CHA-type zeolites with low-cost templates. *Appl. Catal. B Environ.* **2022**, *303*, 120928. [[CrossRef](#)]
22. Zhao, D.; Feng, J.; Huo, Q.; Melosh, N.; Fredrickson, G.H.; Chmelka, B.F.; Stucky, G.D. Triblock Copolymer Syntheses of Mesoporous Silica with Periodic 50 to 300 Angstrom Pores. *Science* **1998**, *279*, 548–552. [[CrossRef](#)] [[PubMed](#)]
23. Oliveira, M.L.M.; Silva, C.M.; Moreno-Tost, R.; Farias, T.L.; Jiménez-López, A.; Rodríguez-Castellón, E. A study of copper-exchanged mordenite natural and ZSM-5 zeolites as SCR–NO<sub>x</sub> catalysts for diesel road vehicles: Simulation by neural networks approach. *Appl. Catal. B Environ.* **2009**, *88*, 420–429. [[CrossRef](#)]
24. Korkkuna, O.; Leboda, R.; Skubiszewska-Zieba, J.; Vrublevs'ka, T.; Gun'ko, V.M.; Ryczkowski, J. Structural and physicochemical properties of natural zeolites: Clinoptilolite and mordenite. *Microporous Mesoporous Mater* **2006**, *87*, 243–254. [[CrossRef](#)]
25. Sacramento, R.A.; Cysneiros, O.M.S.; Silva, B.J.B.; Silva, A.O.S. Synthesis and characterization of mesoporous materials with SBA and MCM structure types. *Cerâmica* **2019**, *65*, 376. [[CrossRef](#)]
26. Yu, R.; Zhao, Z.; Huang, S.; Zhang, W. Cu-SSZ-13 zeolite–metal oxide hybrid catalysts with enhanced SO<sub>2</sub>-tolerance in the NH<sub>3</sub>-SCR of NO<sub>x</sub>. *Appl. Catal. B Environ.* **2020**, *269*, 118825. [[CrossRef](#)]
27. Shishkin, A.; Shwan, S.; Pingel, T.N.; Olsson, E.; Clemens, A.; Carlsson, P.-A.; Härelind, H.; Skoglundh, M. Functionalization of SSZ-13 and Fe-Beta with Copper by NH<sub>3</sub> and NO Facilitated Solid-State Ion-Exchange. *Catalysts* **2017**, *7*, 232. [[CrossRef](#)]
28. Datka, J.; Turek, A.M.; Jehng, J.M.; Wasch, I.E. Acidic properties of supported niobium oxide catalysts: An infrared spectroscopy investigation. *J. Catal.* **1992**, *135*, 186–199. [[CrossRef](#)]
29. Oliveira, M.L.M.; Silva, C.M.; Moreno-Tost, R.; Farias, T.L.; Jiménez-López, A.; Rodríguez-Castellón, E. Simulation of SCR equipped vehicles using iron-zeolite catalysts. *Appl. Catal. A Gen.* **2009**, *366*, 13–21. [[CrossRef](#)]
30. Oliveira, M.L.M.; Silva, C.M.; Moreno-Tost, R.; Farias, T.L.; Jiménez-López, A.; Rodríguez-Castellón, E. Modelling of NO<sub>x</sub> emission factors from heavy and light-duty vehicles equipped with advanced aftertreatment systems. *Energy Convers. Manag.* **2011**, *52*, 2945–2951. [[CrossRef](#)]
31. Moreno-Tost, R.; Oliveira, M.L.M.; Eliche-Quesada, D.; Jiménez-Jiménez, J.; Jiménez-López, A.; Rodríguez-Castellón, E. Evaluation of Cu-PPHs as active catalysts for the SCR process to control NO<sub>x</sub> emissions from heavy duty diesel vehicles. *Chemosphere* **2008**, *72*, 608–615. [[CrossRef](#)] [[PubMed](#)]
32. Koltsakis, G.C.; Stamatelos, A.M. Modeling dynamic phenomena in 3-way catalytic converters. *Chem. Eng. Sci.* **1999**, *54*, 4567–4578. [[CrossRef](#)]
33. Rivera-Garza, M.; Olguín, M.T.; García-Sosa, I.; Alcántara, D.; Rodríguez-Fuentes, G. Silver supported on natural Mexican zeolite as an antibacterial material. *Microporous Mesoporous Mater.* **2000**, *39*, 431–444. [[CrossRef](#)]
34. Shin, Y.; Jung, Y.; Cho, C.P.; Pyo, Y.D.; Jang, J.; Kim, G.; Kim, T.M. NO<sub>x</sub> abatement and N<sub>2</sub>O formation over urea-SCR systems with zeolite supported Fe and Cu catalysts in a nonroad diesel engine. *Chem. Eng. J.* **2020**, *381*, 122751. [[CrossRef](#)]
35. Vasylechko, V.O.; Gryshchouk, G.V.; Kuzma, Y.B.; Zakordonskiy, V.P.; Vasylechko, L.O.; Lebedynets, L.O.; Kalytovs'ka, M.B. Adsorption of cadmium on acid-modified Transcarpathian clinoptilolite. *Microporous Mesoporous Mater.* **2003**, *60*, 183–196. [[CrossRef](#)]
36. Vélez, R.P.; González, M.P.E.; Bentrup, U. Preparation and in situ spectroscopic characterization of Cu-clinoptilolite catalysts for the oxidative carbonylation of methanol. *Microporous Mesoporous Mater.* **2012**, *164*, 93–98. [[CrossRef](#)]
37. Park, J.H.; Park, H.J.; Baik, J.H.; Nam, I.S.; Shin, C.H.; Lee, J.H.; Cho, B.K.; Oh, S.H. Hydrothermal stability of CuZSM5 catalyst in reducing NO by NH<sub>3</sub> for the urea selective catalytic reduction process. *J. Catal.* **2006**, *240*, 47–57. [[CrossRef](#)]
38. Peng, X.; Zhao, Y.; Yang, T.; Yang, Y.; Jiang, Y.; Ma, Z.; Li, X.; Hou, J.; Xi, B.; Liu, H. One-step and acid free synthesis of γ-Fe<sub>2</sub>O<sub>3</sub>/SBA-15 for enhanced arsenic removal. *Microporous Mesoporous Mater.* **2018**, *258*, 26–32. [[CrossRef](#)]
39. Cai, C.; Zhanga, Z.; Zhang, H. Electro-assisted heterogeneous activation of persulfate by Fe/SBA-15 for the degradation of Orange II. *J. Hazard Mater.* **2016**, *313*, 209–218. [[CrossRef](#)]

40. Sun, B.; Li, L.; Fei, Z.; Gu, S.; Lu, P.; Ji, W. Prehydrolysis approach to direct synthesis of Fe, Al, Cr-incorporated SBA-15 with good hydrothermal stability and enhanced acidity. *Microporous Mesoporous Mater.* **2014**, *186*, 14–20. [[CrossRef](#)]
41. Zhu, L.; Qu, H.; Zhang, L.; Zhou, Q. Direct synthesis, characterization and catalytic performance of Al-Fe-SBA-15 materials in selective catalytic reduction of NO with NH<sub>3</sub>. *Catal. Commun.* **2016**, *73*, 118–122. [[CrossRef](#)]
42. Li, J.; Yang, C.; Zhang, Q.; Li, Z.; Huang, W. Effects of Fe addition on the structure and catalytic performance of mesoporous Mn/Al-SBA-15 catalysts for the reduction of NO with ammonia. *Catal. Commun.* **2015**, *62*, 24–28. [[CrossRef](#)]
43. Yan, H.; Qu, H.; Bai, H.; Zhong, Q. Property, active species and reaction mechanism of NO and NH<sub>3</sub> over mesoporous Fe-Al-SBA-15 via microwave assisted synthesis for NH<sub>3</sub>-SCR. *J. Mol. Catal. A Chem.* **2015**, *403*, 1–9. [[CrossRef](#)]
44. Doula, M.K. Synthesis of a clinoptilolite-Fe system with high Cu sorption capacity. *Chemosphere* **2007**, *67*, 731–740. [[CrossRef](#)] [[PubMed](#)]
45. Tsoncheva, T.; Issa, G.; Genova, I.; Dimitrov, M. Formation of catalytic active sites in copper and manganese modified SBA-15 mesoporous silica. *J. Porous Mater.* **2013**, *20*, 1361–1369. [[CrossRef](#)]
46. Giraldo, L.; Gonzalez-Navarro, M.F.; Moreno-Pirajan, J.C. Microcalorimetric Study of the Catalytic Properties of SBA-15 Modified with Cu or Fe for Adsorption/Oxidation of Methyl mercaptane. *Orient. J. Chem.* **2013**, *29*, 1297–1309. [[CrossRef](#)]
47. Arcoya, A.; Gonzalez, J.A.; Travieso, N.; Seoane, X.L. Physicochemical and Catalytic Properties of a Modified Natural Clinoptilolite. *Clay Miner.* **1994**, *29*, 123–131. [[CrossRef](#)]
48. Palacio, R.; Gallego, J.; Gabelica, Z.; Batiot-Dupeyrat, C.; Barrault, J.; Valange, S. Decomposition of ethanol into H<sub>2</sub>-rich gas and carbon nanotubes over Ni, Co and Fe supported on SBA-15 and Aerosil. *Appl. Catal. A Gen.* **2015**, *504*, 642–653. [[CrossRef](#)]
49. Pérez-Ramírez, J.; Mul, G.; Kapteijn, F.; Moulijn, J.A.; Overweg, A.R.; Doménech, A.; Ribera, A.; Arends, I.W.C.E. Physicochemical Characterization of Isomorphously Substituted FeZSM-5 during Activation. *J. Catal.* **2002**, *207*, 113–116. [[CrossRef](#)]
50. Ghasemian, N.; Falamaki, C.; Kalbasi, M.; Khosravi, M. Enhancement of the catalytic performance of H-clinoptilolite in propane-SCR-NO<sub>x</sub> process through controlled dealumination. *Chem. Eng. J.* **2014**, *252*, 112–119. [[CrossRef](#)]
51. Zhang, Y.; Xia, C.; Liu, D.; Zhu, Y.; Feng, Y. Experimental investigation of the high-pressure SCR reactor impact on a marine two-stroke diesel engine. *Fuel* **2023**, *335*, 127064. [[CrossRef](#)]
52. Chmielarz, L.; Kuśtrowski, P.; Dziembaj, R.; Cool, P.; Vansant, E.F. SBA-15 mesoporous silica modified with metal oxides by MDD method in the role of DeNO<sub>x</sub> catalysts. *Microporous Mesoporous Mater.* **2010**, *127*, 133–141. [[CrossRef](#)]
53. Yamamoto, A.; Mizuno, Y.; Teramura, K.; Hosokawa, S.; Tanaka, T. Surface Ba species effective for photoassisted NO<sub>x</sub> storage over Ba-modified TiO<sub>2</sub> photocatalysts. *Appl. Catal. B Environ.* **2016**, *180*, 283–290. [[CrossRef](#)]
54. Liu, C.; Wang, H.; Bi, Y.; Zhang, Z. A study on the selective catalytic reduction of NO<sub>x</sub> by ammonia on sulphated iron-based catalysts. *RSC Adv.* **2020**, *10*, 40948–40959. [[CrossRef](#)]
55. Fan, Y.; Zhang, J.; Yang, L.; Lu, M.; Ying, T.; Deng, B.; Dai, W.; Luo, X.; Zou, J.; Luo, S. Enhancing SO<sub>2</sub>-shielding effect and Lewis acid sites for high efficiency in low-temperature SCR of NO with NH<sub>3</sub>: Reinforced electron-deficient extent of Fe<sup>3+</sup> enabled by Ti<sup>4+</sup> in Fe<sub>2</sub>O<sub>3</sub>. *Sep. Purif. Technol.* **2023**, *311*, 123272. [[CrossRef](#)]
56. Xiao, X.; Xiong, S.; Shi, Y.; Shan, W.; Yang, S. Effect of H<sub>2</sub>O and SO<sub>2</sub> on the Selective Catalytic Reduction of NO with NH<sub>3</sub> Over Ce/TiO<sub>2</sub> catalyst: Mechanism and kinetic study. *J. Phys. Chem. C* **2016**, *120*, 1066–1076. [[CrossRef](#)]
57. Fan, C.; Chen, Z.; Pang, L.; Ming, S.; Zhang, X.; Albert, K.B.; Liu, P.; Chen, H.; Li, T. The influence of Si/Al ratio on the catalytic property and hydrothermal stability of Cu-SSZ-13 catalysts for NH<sub>3</sub>-SCR. *Appl. Catal. A Gen.* **2018**, *550*, 256–265. [[CrossRef](#)]
58. Mohan, S.; Dinesha, P.; Kumar, S. NO<sub>x</sub> reduction behaviour in copper zeolite catalysts for ammonia SCR systems: A review. *Chem. Eng. J.* **2020**, *384*, 123253. [[CrossRef](#)]
59. Wang, P.; Yu, D.; Zhang, L.; Ren, Y.; Jin, M.; Lei, L. Evolution mechanism of NO<sub>x</sub> in NH<sub>3</sub>-SCR reaction over Fe-ZSM-5 catalyst: Species-performance relationships. *Appl. Catal. A Gen.* **2020**, *607*, 117806. [[CrossRef](#)]
60. Xiaoyan, S.; Hong, H.; Lijuan, X. The effect of Fe species distribution and acidity of Fe-ZSM-5 on the hydrothermal stability and SO<sub>2</sub> and hydrocarbons durability in NH<sub>3</sub>-SCR reaction. *Chin. J. Catal.* **2015**, *36*, 649–656. [[CrossRef](#)]
61. Gao, F.; Wang, Y.; Kollár, M.; Washton, N.M.; Szanyi, J.; Peden, C.H.F. A comparative kinetics study between Cu/SSZ-13 and Fe/SSZ-13 SCR catalysts. *Catal. Today* **2015**, *258*, 347–358. [[CrossRef](#)]

**Disclaimer/Publisher's Note:** The statements, opinions and data contained in all publications are solely those of the individual author(s) and contributor(s) and not of MDPI and/or the editor(s). MDPI and/or the editor(s) disclaim responsibility for any injury to people or property resulting from any ideas, methods, instructions or products referred to in the content.